Center for Turbulence Research
Proceedings of the Summer Program 1992

Direct simulation of polymer drag reduction in free shear flows and vortex dipoles

By P. Orlandi[1] G.M. Homsy[2] and J. Azaiez[2]

One of the most efficient techniques for drag reduction is the injection of polymers near a wall which can achieve a reduction in drag up to 80%. Several experimental observations tend to indicate that polymers modify the turbulence structures within the buffer layer and show that the changes consist of a weakening of the strength of the streamwise vortices. In this paper, we investigate the effects of viscoelasticity on two different types of flows: the vortex dipole impinging walls to model streamwise vortices in a turbulent boundary layer and the mixing layer that represents free shear flows. For this purpose, we examined three different rheological models: the Oldroyd-B model, the Jeffrey's corotational model, and the FENE-P model.

1 Introduction

Evidence of drag reduction both by passive and active control has been observed experimentally, but a clear explanation of the mechanisms responsible for this reduction has not been given, mainly because the experimental observations cannot describe all the details of the flow. In the literature, there is a large number of papers devoted to the experimental study of the wall layer structures in drag reducing flows. This literature is summarized in the review article of Tiederman (1989). The main conclusion that we can draw from these papers is that drag reduction is due to modifications of the wall layer structures, particularly in the buffer region, the most active region in wall bounded flows. From flow visualizations, Oldaker and Tiederman (1977) concluded that the polymer solution inhibits the formation of low speed streaks and that, when these are formed, their spacing in wall coordinates increases with polymer concentration.

In the last decade, direct simulations of wall bounded flows have been a very useful tool for a deeper understanding of turbulence structures and their role in wall friction. Free shear flows of viscoelastic fluids on the other hand, have not received as much attention as bounded flows did, and to our knowledge, only few and inconclusive experiments have been conducted.

Due to the lack of a universal constitutive equation that describes most common viscoelastic behaviors, numerical studies of non-Newtonian fluids have been limited to special types of polymeric solutions in simple flows. In spite of these limitations, many results showing important effects of viscoelasticity for different types of flows have been reported (Tiederman(1989)). In a previous paper (Orlandi 1991), a

1 Università di Roma, "La Sapienza"
2 Stanford University

heuristic relation between the polymer stresses and the flow properties in a channel flow was used to investigate how the flow structures change in a situation where drag reduction was achieved. The model was not tensorial invariant and was not related to the molecular structure of the polymers.

In this paper, we wish to initiate a systematic study of the effects of polymers on the flow structures using rheological models based on transport equations for the stresses of the polymers. In particular, we studied the case of vortex dipole in the presence of walls. A vortex dipole models the streamwise vortices in the buffer region of a turbulent channel, which are responsible for turbulence production and turbulent drag. This was shown numerically in a quasi two-dimensional simulation by Orlandi and Jimenez (1991). We have also examined the case of the roll-up of a two-dimensional mixing layer. Our interest in the mixing layer problem was motivated by the results of linear stability analysis reported by Azaiez and Homsy (1992). This analysis shows that, in a special limit of the elasticity number, viscoelasticity reduces the instability of the flow.

We considered three viscoelastic models: the Jeffrey's corotational model, the Oldroyd-B model, and the FENE-P model which describes the rheological properties of dilute polymeric solutions. The flows governed by these rheological models are characterized by three dimensionless numbers: The Reynolds number, Re, the Weissenberg number, We, a dimensionless measure of the elasticity of the fluid and the coefficient $K = \dfrac{\eta_S}{\eta_S + \eta_P}$, a ratio of the solvent viscosity η_S and the polymeric contribution to the shear viscosity, η_P. In the case of the FENE-P model, a third parameter, b, related to the nature of the spring used to model the macromolecule, is introduced.

The first interesting physical aspect that comes out of the study of these three models is that the formation of small scales is enhanced and that these small scales are rapidly dissipated. This unexpected phenomenon needs an experimental confirmation, and we hope that in the near future two-dimensional experiments will be performed in order to both understand in details the behavior of dilute polymeric solutions and validate the results of our two-dimensional viscoelastic simulations.

While for the mixing layer we obtained results in a quite large range of the Weissenberg number, only results at small Weissenberg numbers could be obtained for dipoles impinging walls because of the special flow topology: with the FENE-P model, the polymeric stresses reached very large values at the stagnation point, and the calculations were diverging for We of order 1. At smaller values of We, the calculations did not differ from the Newtonian case because the flow stresses were able to overcome any possible polymeric effect.

2 Physical and numerical model

We used a vorticity-streamfunction formulation for the Cauchy's momentum equation. This equation is closed through evolution equations relating the stress tensor to the shear rate tensor. In all the subsequent analysis, the stress tensor is written as the sum of two stresses.

$$\tau_{ij} = \eta(K\dot{\gamma}_{ij} + (1-K)a_{ij}) \tag{1}$$

We fixed $K = 0.5$.

The first term in Eq.(1) reflects the contribution of the Newtonian solvent and is proportional to the shear rate tensor $\dot{\gamma}$, the second one represents the polymeric contribution and is proportional to the tensor a. The tensor a satisfies different evolution equations corresponding to the various rheological models we are examining.

Eq.(1) leads to the following vorticity equation

$$\frac{\partial \omega}{\partial t} = -J(\omega,\psi) + \frac{k}{Re}\nabla\omega + \frac{1-k}{Re}\left(\frac{\partial a_{12}}{\partial x_1^2} - \frac{\partial a_{12}}{\partial x_2^2} - \frac{\partial a_{11}-a_{22}}{\partial x_1 \partial x_2}\right) \tag{2}$$

where the nonlinear terms have been expressed as a Jacobian. The streamfunction is evaluated from the Poisson's equation $\nabla^2\psi = -\omega$.

In the case of the mixing layer, we imposed periodic conditions in the streamwise direction. In the transverse direction, free slip conditions are imposed in the finite difference code while periodic conditions are imposed for the spectral code. In the case of the spectral code, the domain was made large enough in the transverse direction to ensure that all functions go to zero at the periphery of the domain. Non-slip conditions are imposed at the wall for the vortex dipole.

The stresses are governed by a set of partial differential equations which constitute the rheological model. We have considered several models: the first one is the Jeffrey's corotational model which is obtained by formulating the equations of state in a frame translating with the fluid and rotating with the local angular velocity of the fluid. The equation describing this model is:

$$a_{ij} + We\frac{\tilde{D}a_{ij}}{\tilde{D}t} = \dot{\gamma}_{ij} \tag{3}$$

where $We = \dfrac{U\lambda}{\delta}$ is the Weissenberg number.

$$\frac{\tilde{D}a_{ij}}{\tilde{D}t} = \frac{Da_{ij}}{Dt} + \omega_{ik}a_{kj} + \omega_{jk}a_{ik} \tag{4}$$

is the Jaumann derivative.

The rheological equation for the Oldroyd-B model is:

$$a_{ij} + We\frac{\delta a_{ij}}{\delta t} = \dot{\gamma}_{ij} \tag{5}$$

The upper convective derivative $\dfrac{\delta a_{ij}}{\delta t}$ is related to the Jaumann derivative through the relation:

$$\frac{\delta a_{ij}}{\delta t} = \frac{\tilde{D}a_{ij}}{\tilde{D}t} + \frac{1}{2}(a_{ik}\dot{\gamma}_{kj} + \dot{\gamma}_{ik}a_{kj}) \tag{6}$$

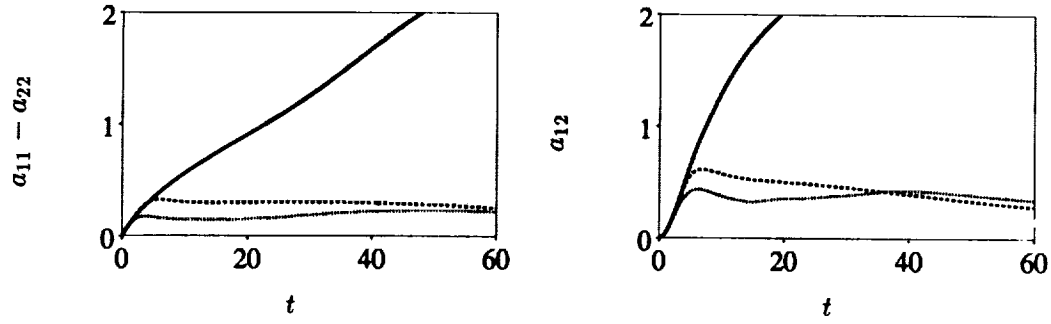

FIGURE 1. Time evolution of the polymeric stresses at $We = 5$. —— Oldroyd; ... Jeffreys; ---- FENE-P

To the contrary of what is observed for the Jeffrey's model, the Oldroyd-B model has a very large dependence on the Weissenberg number as will be discussed in the next paragraph. We found that at certain values of We, the stresses grow indefinitely in time and the growth rate is flow dependent.

The Oldroyd-B model gives a steady state elongational viscosity that goes to infinity at a finite elongational rate. This unlikely behavior results because the Hookean dumbbell model permits infinite extension. In order to avoid this unrealistic behavior, a Warner law is used instead of the Hook law leading to the FENE-P model. This model is described by Mackay and Petrie (1989) and the rheological equation is:

$$a_{ij}Z + We\frac{\delta a_{ij}}{\delta t} = \dot{\gamma}_{ij} + \frac{DlnZ}{Dt}(\mathbf{I} + a_{ij}We) \tag{7}$$

where $Z = 1 + \frac{n}{b}(1 + \frac{We}{n}a_{ii})$, $n = 2$ for a two dimensional flow. In order to facilitate the numerical solution of Eq.(7), $\frac{DlnZ}{Dt}$ was derived from the transport equation for a_{ii}.

The set of governing equations have been discretized by a finite difference scheme second order accurate in space and in time. The main characteristics of the numerical method is that it discretizes $J(\omega, \psi)$ by the Arakawa scheme which conserves energy, enstrophy, and skew symmetry in the inviscid limit. The polymer contribution to the stresses have been located at different grid positions with a_{11} and a_{22} at the center of the cell and a_{12} at the same location of ω and ψ. This choice allows a very compact formulation of the right hand side of Eq. (2) and leads to the solution without imposing boundary conditions for a_{11} and a_{22}. On the other hand, a_{12} has been taken equal to zero both on free-slip and no-slip walls. The stream function has been solved directly by using the Fourier transform in the periodic direction. Numerical simulations have been performed on the CRAY YMP84 at NASA Ames and the CPU required for 1000 time steps on a 128×128 grid was 150 seconds.

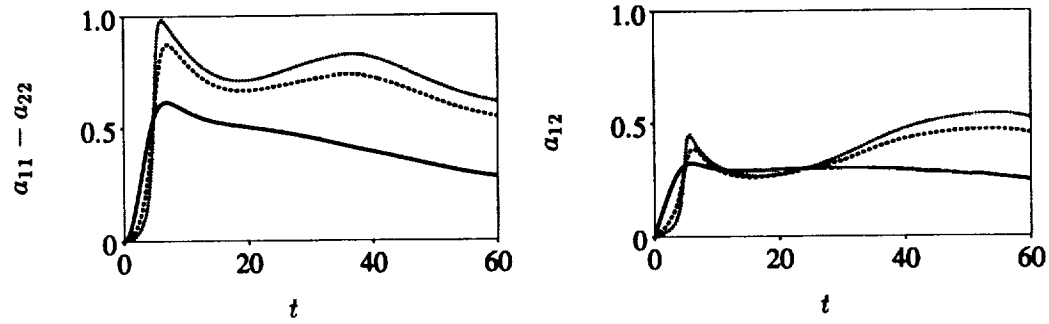

FIGURE 2. Time evolution of the polymeric stresses at $b = 5$. —— $We = 5$; ---- $We = 20$; ... $We = 50$

3 Results

1 Mixing layer

The mixing layer simulations have been performed in order to study the effects of viscoelasticity on the vorticity field. Numerical simulation using a pseudospectral method were performed in order to compare with the finite difference results. The good comparison between finite difference and pseudospectral simulations will be presented elsewhere.

The initial base state is given by a hyperbolic tangent velocity profile on which we superposed a *cos* perturbation on the stream function with the maximum at the centerline $y = 0$. The most unstable wave number, $\alpha = 0.44$, has been used in all the simulations. The extension of the domain in the streamwise direction is set to $\frac{2\pi}{\alpha}\delta$ with δ the momentum thickness of the mixing layer. The vertical extension has been heuristically fixed equal to 8δ. The Reynolds number is defined as $Re = \frac{\delta u_0}{\nu}$ where $u_0 = (U_1 - U_2)/2$. U_1 and U_2 are the free-stream velocities.

The growth of the maximum value of($a_{11} - a_{22}$) and of a_{12} obtained for the three viscoelastic models are shown in Fig. 1. At $We = 5$, the stresses are smaller for the Jeffrey's corotational model than for the other two models; as a consequence, the vorticity field does not differ appreciably from the Newtonian case. In the case of the Oldroyd-B model, the stresses grew rapidly due to the unrealistic characteristic of this model that allows the macromolecules to extend infinitely.

We suspected that the divergence of the codes for the Oldroyd-B model at high We to result from some numerical instability. By refining the mesh and varying the time step for both the finite difference and the pseudospectral codes, we found that, at the same values of We, the solution was always diverging at the same point in time. We have shown that the divergence was caused by the change of sign of the eigenvalues of the system of nonlinear equations. The change of sign occurred at certain values of We, and this value is flow dependent.

In the case of the FENE-P model, the dependence of the flow on the Weissenberg number and on the parameter b has been studied by performing different simulations

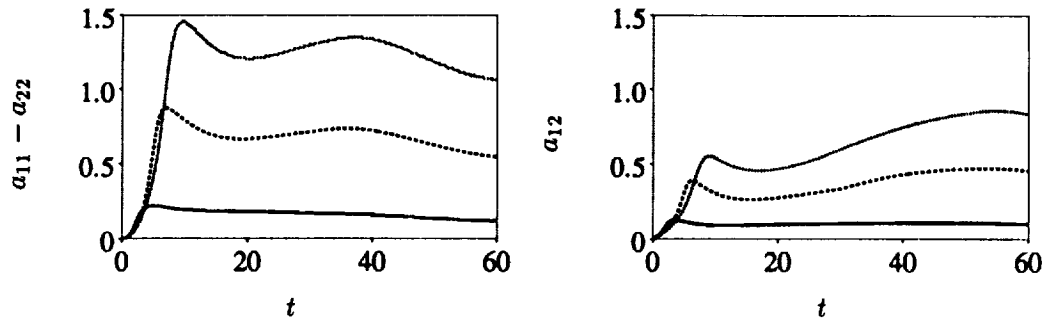

FIGURE 3. Time evolution of the polymeric stresses at $We = 20$. —— $b = 1$; ---- $b = 5$; ... $b = 10$

for the mixing layer at $Re = 100$. Fig. 2 shows how the polymeric contribution to the stresses depend on We at $b = 5$. The simulations at $We = 5$ and $We = 20$ were performed on a 128×128 grid. With this grid, at $We = 50$, the high values of the stresses produced wiggles in the vorticity field at $t \approx 40$; these wiggles partially persisted with a grid twice finer and disappeared with a 384×384 grid. Fig. 2 also shows that the effect of the Weissenberg number on a_{12} are large at later times and that large variations of the maximum value of($a_{11} - a_{22}$) occur at low rather than at high We values. Fig. 2 shows also that by increasing the Weissenberg number from $We = 20$ to $We = 50$, the variations are less important than those obtained by taking the We from 1 to 20.

Fig. 3 shows the dependence on the parameter b. We notice that the maxima are more dependent on b than on We and that the maximum values are higher than those observed in Fig. 2. This behavior is consistent with the fact that for very large values of b the Oldroyd-B model is recovered.

A clear picture of the evolution of the flow is obtained from the analysis of the vorticity and of the stress field . Vorticity contour plots at three different times and for three different We values are presented in Fig. 4. We remark that at low We, the flow does not differ from the Newtonian case while at higher We, more noticeable changes appear in the structure of the mixing layer. Very interesting is the occurrence of intense gradients in the braids. These gradients are convected in the roll-up region and persist for a longer time, producing a faster and more intense roll-up as shown at $We = 50$.

$a_{11} - a_{22}$ is the other quantity contributing to the modification of the vorticity field and can be measured experimentally. Fig. 5 shows a large increase of its maximum value when We goes from $We = 1$ to $We = 20$. On the other hand, when the Weissenberg number increases from $We = 20$ to $We = 50$, the value does not change significantly, then we can expect minor changes in the vorticity field. From Fig. 4 and Fig. 5 we can draw a first conclusion that the effect of the Weissenberg number is to concentrate the modifications by polymers at small scales. From contour plots of vorticity and $a_{11} - a_{22}$, not reported in this paper, we have observed that by increasing b, high peak values are produced and are localized in

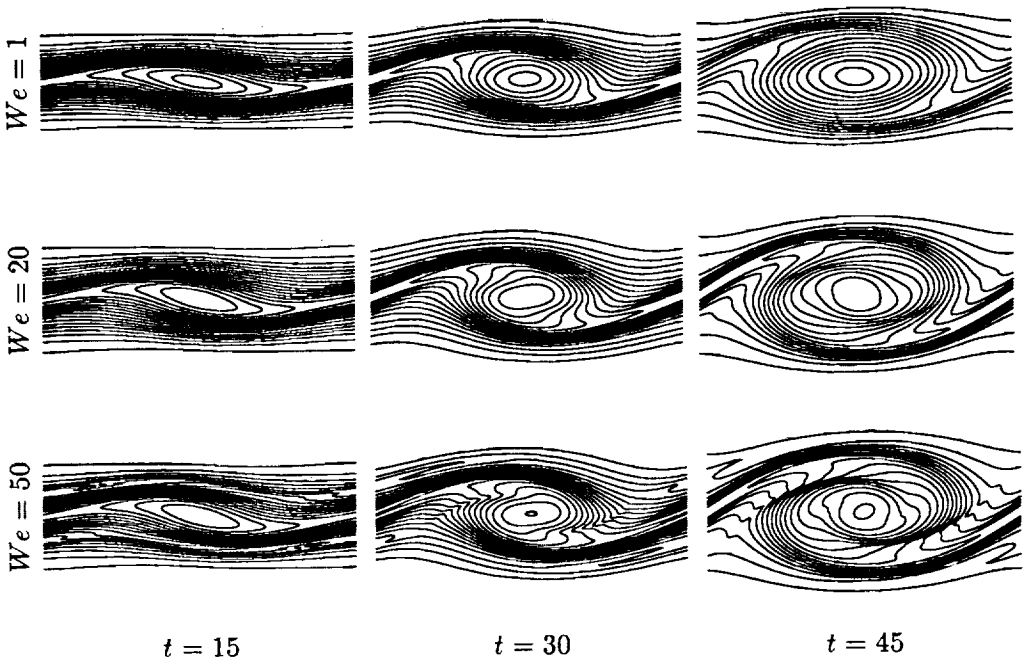

FIGURE 4. Vorticity contour plots. b=5.

wider regions, and thus weaker effects on the mixing layer roll-up are observed.

At this stage of the work and without having any experimental observations with which to compare our results, we do not wish to go into a deeper analysis of the flow to understand the mechanisms responsible for this rapid transfer of energy from the large scales to the smaller scales. We think that the results we obtained will be of more interest if they can be checked through experimental studies. The comparison between numerical and experimental predictions will help in understanding the physics behind the effects of viscoelasticity on the structure of the flow.

2 Vortex dipole impinging walls

This two-dimensional flow has been considered because it represents the streamwise vortices in a turbulent boundary layer, which are responsible of turbulent drag and turbulence production. In the present two-dimensional simulation, we have introduced a Lamb dipole rather than a single vortical structure because the dipole moves towards the wall by self-induction while a single vortex must be advected towards the wall by an external field. As a first case, we have considered the interaction with a free-slip wall to investigate the distributions of the polymeric contribution to the stresses generated at the moment of the impact. We expect that, at the stagnation point, a large increase of the polymeric stresses is obtained since this is a point where strong elongations of the polymers molecule occur. This large increase of the polymers stresses is the cause of the difficulty to perform simulations at high Weissenberg numbers.

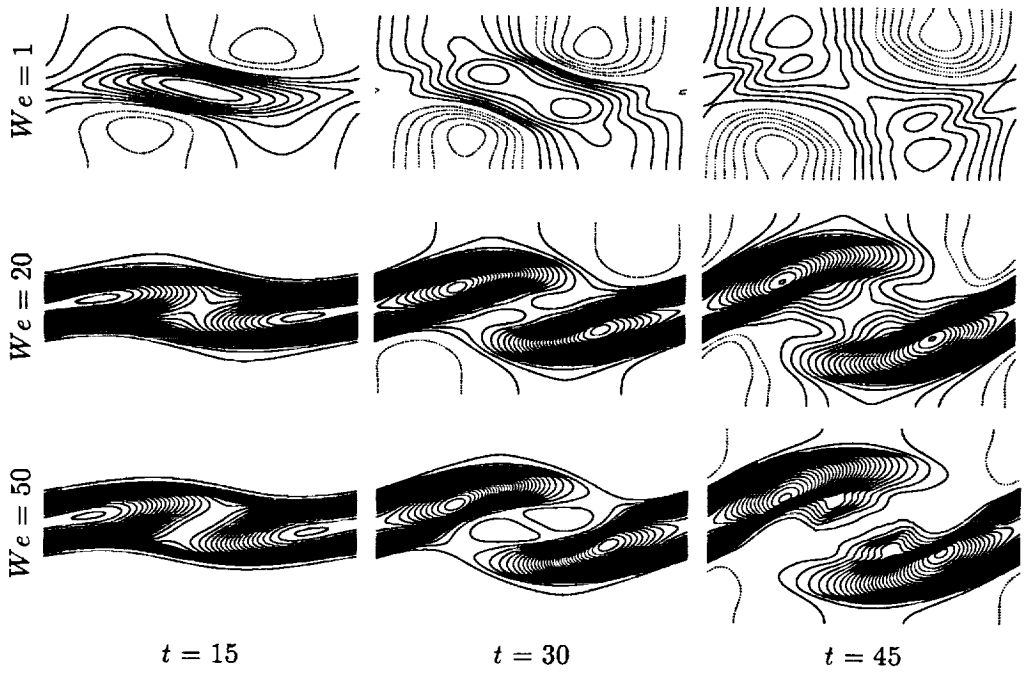

FIGURE 5. $a_{11} - a_{22}$ contour plots. b=5.

The simulations were performed on a 192×192 grid points in a domain extending in the horizontal and in the vertical directions 4 dipoles radii. Solutions with the FENE-P model were obtained only for $We \leq 3$ and $b \leq 1$ at $Re = \frac{U_d a}{\nu} = 50$ (U_d is the translation velocity of the dipole, a is the dipole radius). The simulations were performed both with free-slip and no-slip walls. In the case of the dipole impinging a free-slip wall, the vorticity field, at the moment of the impact, is shown in Fig. 6. Similarly to what has been observed in the mixing layer, this figure shows that $a_{11} - a_{22}$ increases more than a_{12}; the maximum values are reached in the region of maximum normal stress and low vorticity. Although large polymeric stresses are obtained, the dipole does not change their shape appreciably, and this could be a consequence of the fact that dipolar structures are very stable to large perturbations.

When the dipole impinges a non-slip wall, Fig. 7 shows that the vorticity field does not depend strongly on the Weissenberg number. There is, however, a slight decrease of the magnitude of the vorticity level as compared to the Newtonian case, but this decrease is not sufficient to change the type of vortex rebound. We did not perform a systematic study of the We effects.

4 Conclusion

This preliminary study testing different viscoelastic models allowed us to predict the effects of the introduction of polymers on the flow structure. By comparing

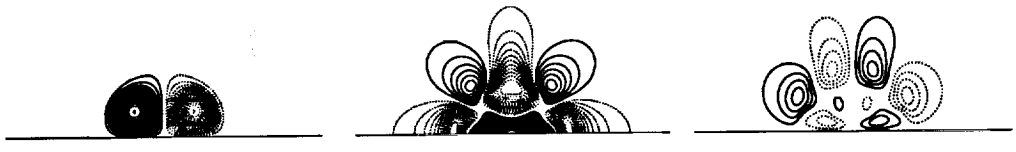

FIGURE 6. Contour plots of *(a)* vorticity, *(b)* $a_{11} - a_{22}$ and *(c)* a_{12} for dipole impinging a free-slip wall at $Re = 50$, $We = 2$ and $b = .4$.

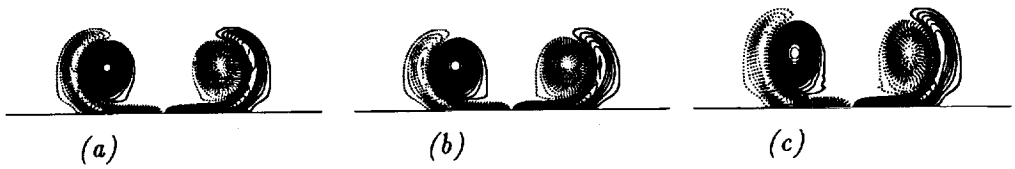

FIGURE 7. Vorticity Contour plots *(a)* newtonian, *(b)* $We = .5, b = 1.$ and *(c)* $We = 3., b = 1.$ for dipole impinging a non-slip wall at $Re = 50$.

the solutions obtained by the finite difference scheme and those obtained by a pseudospectral method, we have shown that the solutions did not diverge in time for numerical reasons. Two-dimensional simulations revealed that the cause of the exponential growth in the Oldroyd-B model at certain We is caused by a change in the sign of the eigenvalues of the a_{11} stress equation.

Using the FENE-P model, we were able to conduct numerical simulations at reasonably high Weissenberg numbers. In the case of the mixing layer, we noticed some changes in the structures of the roll-up. This is an interesting phenomenon since, in a space developing mixing layer just after the splitter plate, the initial instability could influence the growth of the mixing layer. The present simulations show the large potential in using polymers for the control and possibly the modification of the structures of the mixing layer. We hope to pursue this study by examining the effects of polymers on vortex stretching and streamwise vortices in the mixing layer. In the case of the vortex dipole, the changes on the vorticity field are negligible.

We believe that the results reported in this study should be pursued by more detailed simulations and by experimental studies that will help in understanding the mechanisms responsible for the changes observed in the case of the mixing layer with the FENE-P model. We hope that the present study will stimulate more interest in non- Newtonian flows among both theoreticians and experimentalists.

REFERENCES

AZAIEZ J., & HOMSY G. M. 1992 Linear stability of free shear flows of viscoelastic liquids. Submitted to *J. Fluid Mech.*

LUMLEY J. L. 1971 Applicability of the Oldroyd constitutive equations to flow of dilute polymer solutions. *Phys. of Fluids.* **14**, 2282-2284

MACKAY, M. E. & PETRIE, S. J. 1989 Estimates of apparent elongational viscosity using the fibre spinning and pure methods calculations for a FENE-P

dumbbell model and comparisons with published data. *Rheological Acta.* **28**, 281-293

OLDAKER, D. K. & TIEDERMAN W. G. 1977 Spatial structures of the viscous sublayer in a drag-reducing channel flows. *Phys. Fluids.* **20**, S133-S144

ORLANDI, P. 1991 A tentative approach to the direct simulation of drag reduction by polymers. *Bulletin of the American Physical Society.* **36**(10), 2709

ORLANDI, P. & JIMENEZ, J. 1991 A model for bursting of near wall vortical structures in boundary layers. *Proceeding of 8th Symposium on Turbulent Shear Flows*, Munchen.

TIEDERMAN W. G. 1989 The effect of dilute polymer solutions on viscous drag and turbulence structure. Proceedings of the second IUTAM symposium on structure of turbulence and drag reduction. A. Gyr (editor) Springer-Verlag.